



Trans. Nonferrous Met. Soc. China 31(2021) 2024-2038

Transactions of **Nonferrous Metal** Society of China





Effect of multi-pass multi-directional forging on tribological properties of Si-rich eutectoid ZA alloys

D. YOUSEFI, R. TAGHIABADI, M. H. SHAERI

Department of Materials Science and Metallurgy, Imam Khomeini International University, Qazvin, Iran

Received 7 July 2020; accepted 18 January 2021

Abstract: The effect of multi-pass multi-directional forge (MDF) on the tribological properties of ZA22-xSi alloy (x=0, 4, 8 wt.%) was investigated. The results indicate that MDF breaks down the cast microstructure of alloys and produces a well-modified microstructure comprising finely distributed α - and η -phases and primary Si particles. It is also found that, despite the matrix work softening, MDFed ZA22-xSi alloys show high wear resistance. The maximum wear resistance is observed in the five-pass MDFed ZA22-4Si sample, at the applied loads of 10 and 30 N, and its wear rates are lower than the wear rate of the as-cast ZA22 alloy by about 80% and 75%, respectively. MDF also significantly decreases both average friction coefficient and friction coefficient fluctuation of the sample. The high resistance of the substrate to microcracking, formation of hard Si reinforcements, fine redistribution of α - and η -phases in the microstructure, and formation of tribolayers rich in Al and Zn oxides can be considered as the main factors improving the tribological properties.

Key words: multi directional forge (MDF); Zn-22Al alloy; silicon; tribology

1 Introduction

Adding appropriate amounts of Si to the Zn-Al based alloys (also known as ZA alloys) improves their hardness, strength, and thermal stability. Si-containing ZA alloys also exhibit better wear properties than binary Zn-Al alloys [1-3]. This is due to the formation of hard primary Si particles within a relatively tough matrix. These hard particles increase the overall hardness of the matrix limiting the adhesion between contacting asperities [4,5], and act as load-bearing elements dispersing the applied load [5,6]. Silicon has been also found to be an interesting candidate for partial or complete replacement of Cu, as a common alloying element [7], in ZA-based alloys. This is because Si can improve the hardness and tensile strength of ZA-based alloys without impairing their dimensional stability [8-10]. However, due to the

very low solid-solubility of Si in Zn–Al matrix [11], it mostly precipitates as discrete nearly-pure Si particles with irregular shapes and weak faceted interface within the matrix [12,13]. At low concentrations, Si particles mostly precipitate as eutectic Si in the matrix of Zn-Al alloys improving hardness. However, above concentration, which depends on chemistry and processing condition, the formation of coarse irregular-shaped primary Si particles is likely to impair the mechanical and tribological properties of the alloy [1,3].

SAVASKAN and **BICAN** [1] PRASAD [14] studied the effect of Si on sliding wear behavior of Zn-40Al and Zn-37.5Al alloys and found that, if the Si content exceeds 2.0 wt.%, the formation of coarse brittle primary Si particles in the microstructure deteriorates the alloy wear resistance. However, LIU et al [15] showed that the wear resistance and antifriction capacity of asspray-deposited ZA27–5Si alloy are superior to those of conventionally cast ZA27 alloy. They attributed this to the fine and even distribution of primary Si phases in the microstructure and development of lamellar eutectoid phase with improved interfaces with Si particles. Therefore, to take the advantages of high Si content in ZA alloy series, it seems necessary to refine the coarse Si particles and improve their distribution within the matrix.

Severe plastic deformation (SPD) is one of the most promising approaches which can be used to modify/refine the as-cast microstructure of alloys. During SPD, the bulk material experiences ultra-high strains without a net change of shape. The severe plastically-deformed materials exhibit interesting/unique properties that are not usually observed in conventionally-deformed grained materials [16,17]. Among various SPD techniques, multidirectional forging (MDF) [18], is a simple, cost-effective, and easy-to-use process that can be used to develop fine microstructures in relatively large bulk samples [19]. In this process, a rectangular parallelepiped specimen with different dimensions is successively pressed at different directions $(X \rightarrow Y \rightarrow Z \rightarrow X \rightarrow \cdots)$ [20,21]. Compared to some SPD processes such as equal channel angular pressing (ECAP) and high-pressure torsion (HPT), MDF produces lower strain homogeneity in a processed sample, but it is regarded as an appropriate technique for developing sound refined microstructures in **HCP** alloys deformation capability [19-23]. Moreover, despite high levels of applied strains, MDFed specimens do not experience substantial changes in their cross-section [22].

A review of the literatures indicates that a limited number of studies have been conducted on the effect of MDF on the mechanical behavior of cast ZA alloys [18,22,24]. However, to the best of our knowledge, there is no study investigating the effect of MDF on wear behavior of ZA alloys. Therefore, this study was conducted to investigate

the effect of multi-pass MDF on dry sliding wear resistance and friction behavior of eutectoid Zn–22Al alloy containing 4 wt.% and 8 wt.% Si. It has been shown that multi-pass MDF has a great capability in improving the tribological properties of Si-rich eutectoid Zn–22Al alloys which are also known as Si_P/ZA22 in-situ composites.

2 Experimental

The primary Zn-22Al ingots were produced by using commercially pure Zn (99.5 wt.%) and highly-pure Al (99.9 wt.%). The primary raw materials were melted in SiC crucible using a resistance furnace (AZAR-VM2L1200). After melting the primary charge materials, the required amount of Si was added to the melt using Al-30Si master alloy at 660 °C and the melt was stirred gently for 5 min to ensure complete melting of the master alloy. Thereafter, the melt was poured into a preheated cast-iron mold (250 °C) at 620 °C to obtain slabs with dimensions of 150 mm × $100 \text{ mm} \times 10 \text{ mm}$. The chemical composition of the experimental alloys, analyzed by X-ray fluorescence spectrometer ("ARL ADVANT XP"), is shown in Table 1.

The MDF split die with a central cavity of 40 mm × 15 mm ×10 mm made of hardened and tempered AISI H13 hot-work tool steel ((58±2) HRC) was used for MDF deformation. Its geometrical details have been presented in Ref. [19]. A hydraulic press with a capacity of 100 t, equipped with a resistance furnace, was used to isothermally forge the rectangular parallelepiped samples with dimensions of 10 mm × 10 m ×15 mm at 100 °C with a ram speed of 0.5 mm/s by up to five passes. The imposed strain in each pass of MDF (about 0.47) was calculated by [19]

$$\varepsilon = \frac{2}{\sqrt{3}} \ln \frac{H}{W} \tag{1}$$

where H and W are the height and width of the sample, respectively.

Table 1 Chemical composition of base and Si-containing alloys (wt.%)

Alloy	Code	Al	Si	Fe	Mg	Pb	Sn	Cu	Zn
Zn-22Al	Base-AC	21.30	< 0.01	0.03	0.002	0.005	0.006	0.002	Bal.
Zn-22Al-4Si	4Si-AC	22.43	3.86	0.02	0.002	0.004	0.005	0.002	Bal.
Zn-22Al-8Si	8Si-AC	21.22	7.75	0.04	0.002	0.004	0.006	0.002	Bal.

After each pass of MDF, the sample was rotated 90° around its Z and X-axis, respectively (Fig. 1(a)), and the die and the sample were lubricated by a graphite-based lubricant, i.e. Moly Coat 1000 Paste. The MDFed samples are indicated by xP code following their code number shown in Table 1 (x: number of MDF passes).

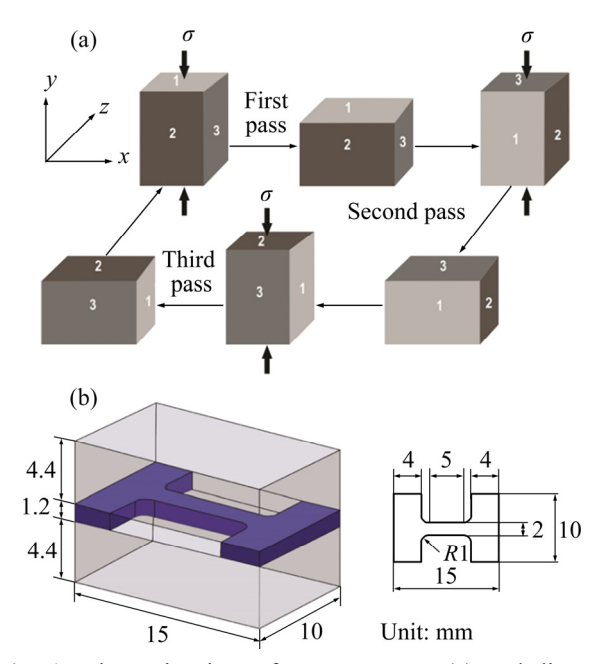


Fig. 1 Schematic view of MDF process (a) and die cut mold, geometry and dimensions of tensile testing specimens (b) [19]

The samples for metallography purpose were prepared by standard metallographic procedures and then were etched using a 2% HF reagent (2 mL HF and 98 mL distilled water) for 10 s to reveal their microstructure. The microstructural observation was performed using a Mira3-XMU Tescan field emission scanning electron microscope (ESEM) equipped with an energy dispersive spectroscopy (EDS) device to perform phase microanalysis. Quantitative metallography was performed by Digimizer 5.3.5 software. The average size (Ferret's diameter) of the Si particles was also measured by dividing the "convex hull perimeter" of the primary Si particles by π [25]. At least 100 particles were analyzed for each sample.

The Vickers microhardness testing was performed by using an HVS-1000A microhardness tester at the closest zone to the center of samples' cross-section under the applied load of 500 g for a dwelling time of 15 s. The average value of six indentations was reported as the final value. The

Brinell hardness test was also carried out under a load of 187.5 kg using a 2.5 mm steel ball to determine the macrohardness of samples. The test was conducted on eight locations and the average value was taken as the final value. The tensile test specimens with the dimensions shown in Fig. 1(b) were wire cut from the MDF processed zone. The tensile tests were performed using a Zwick/Roell-Z100 universal tensile machine at the constant crosshead speed of 0.1 mm/min. The average of three results was reported as the final value. The Archimedes's principle was applied to determining the porosity level of the samples as described comprehensively elsewhere [26].

3 Results and discussion

3.1 Microstructure characterization

The as-cast (AC) microstructures of base-AC and 8Si-AC alloys are shown in Fig. 2. As seen, the microstructure of base-AC alloy consists of two distinct regions: (1) bright gray region comprising Zn-rich η -phase and dark gray $\alpha + \eta$ islands, and (2) light gray dendritic region (lamellar eutectoid colonies of α - and η -phases). A detailed explanation regarding the evolution of cast microstructure in the ZA22 alloy is found in our previous work [27]. The EDS line analyses (Fig. 3) demonstrate the presence of Al- and Zn-rich regions in the microstructure of base-AC sample. Moreover, the EDS analyses of the main alloy microconstituents (see Fig. 2(b)) are shown in Table 2.

Due to its limited solid-solubility in the Zn–Al matrix [11], adding Si to the alloy leads to the formation of irregular shaped Si particles in the microstructure (Fig. 4). The as-cast microstructures of 4Si-AC and 8Si-AC alloys are shown in Figs. 4(c) and (e), respectively. According to the EDS analysis shown in Table 2, increasing the Si content increases both average size and volume fraction of black Si particles in the microstructure. Applying MDF significantly affects the as-cast microstructures. The effects of five-pass (5P) MDF on the microstructure of base-AC, 4Si-AC, and 8Si-AC alloys are shown in Figs. 4(b), (d), and (f), respectively. As seen, as a result of large shear strains applied during this process, the initial dendritic network of the samples has been broken down, the α - and η -phases have been effectively refined and mixed, the Si particles (in Si-containing

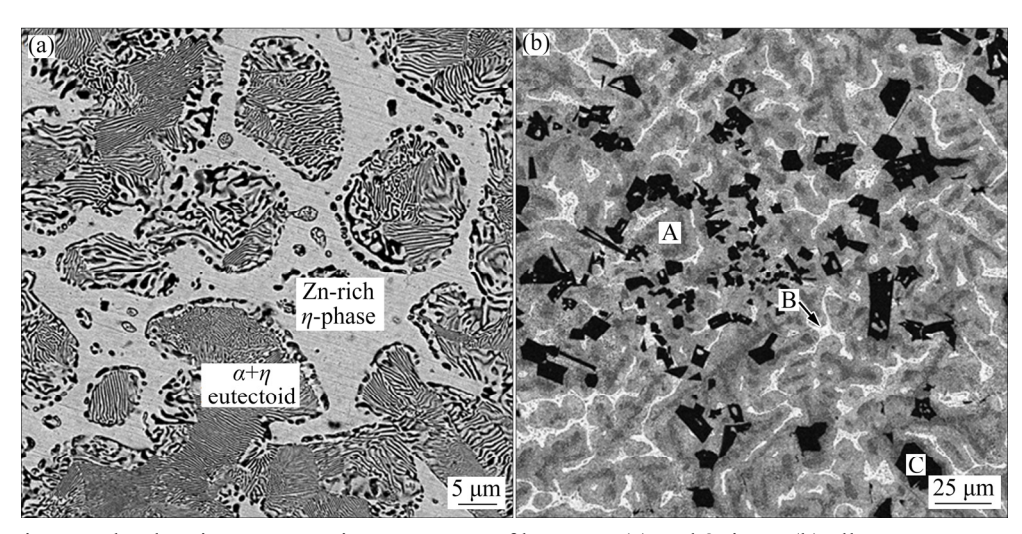


Fig. 2 SEM micrographs showing as-cast microstructures of base-AC (a) and 8Si-AC (b) alloys

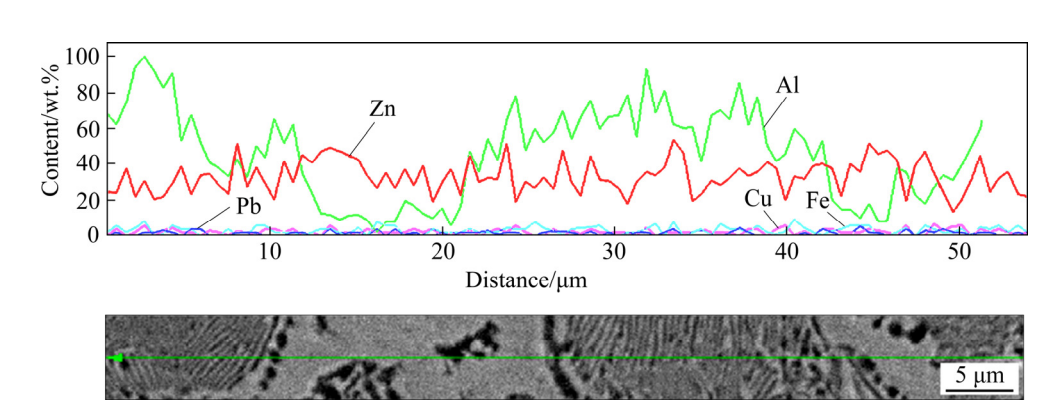


Fig. 3 EDS line analyses showing distribution of Zn- and Al-rich regions in microstructure of base-AC alloy

Table 2 EDS analyses of regions marked on micrograph in Fig. 2(b) (wt.%)

Region	Zn	Al	Si
A	99.7	0.3	0.0
В	73.4	26.6	0.00
C	2.0	1.2	96.8

alloys) have been fractured, their distribution within the matrix has been improved, and the existing micropores have been mostly forged. According to the image analysis results, the average size of primary Si particles decreases from 25.0 and 30.4 μm in 4Si-AC and 8Si-AC alloys to less than about 8.1 and 7.3 μm in 4Si-5P and 8Si-5P alloys, respectively. Moreover, the volume fraction of micropores decreases from 0.78%, 1.46% and 2.17% in base-AC, 4Si-AC and 8Si-AC alloys to about 0.21%, 0.41% and 0.92% in base-5P, 4Si-5P and 8Si-5P alloys, respectively. It is worth noting that the existing micropores are mainly shrinkage-driven one forming as a result of lack of

interdendritic feeding in the last stage of solidification and/or blockage of feeding channels by the coarse primary Si particles as reported elsewhere [27].

3.2 Mechanical properties

The effect of multi-pass MDF on hardness and tensile properties of the experimental samples is shown in Fig. 5. As seen, regardless the presence or absence of Si in the composition, MDF decreases the strength (Fig. 5(a)) and hardness (Fig. 5(d)) of the alloys, but improves their fracture strain (Fig. 5(b)) and toughness (Fig. 5(c)). Increasing the number of MDF passes progressively lowers the hardness/strength, but enhances the ductility. For instance, the microhardnesses of base-5P, 4Si-5P, and 8Si-5P samples are lower than those of base-AC, 4Si-AC, and 8Si-AC samples by 41%, 30%, and 37%, respectively. Moreover, the fracture strains of base-5P, 4Si-5P, and 8Si-5P samples are higher than those of base-AC, 4Si-AC, and 8Si-AC by about 365%, 150%, and 130%, respectively.

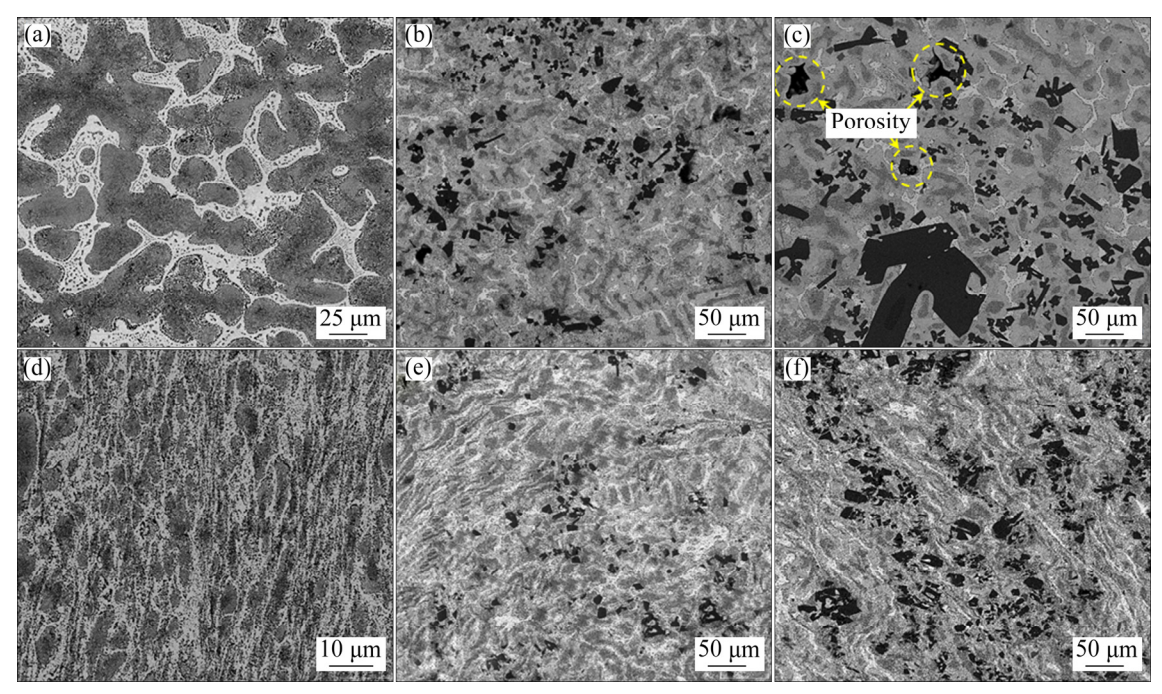


Fig. 4 SEM images of base-AC (a), base-5P (b), 4Si-AC (c), 4Si-5P (d), 8Si-AC (e), and 8Si-5P (f) samples

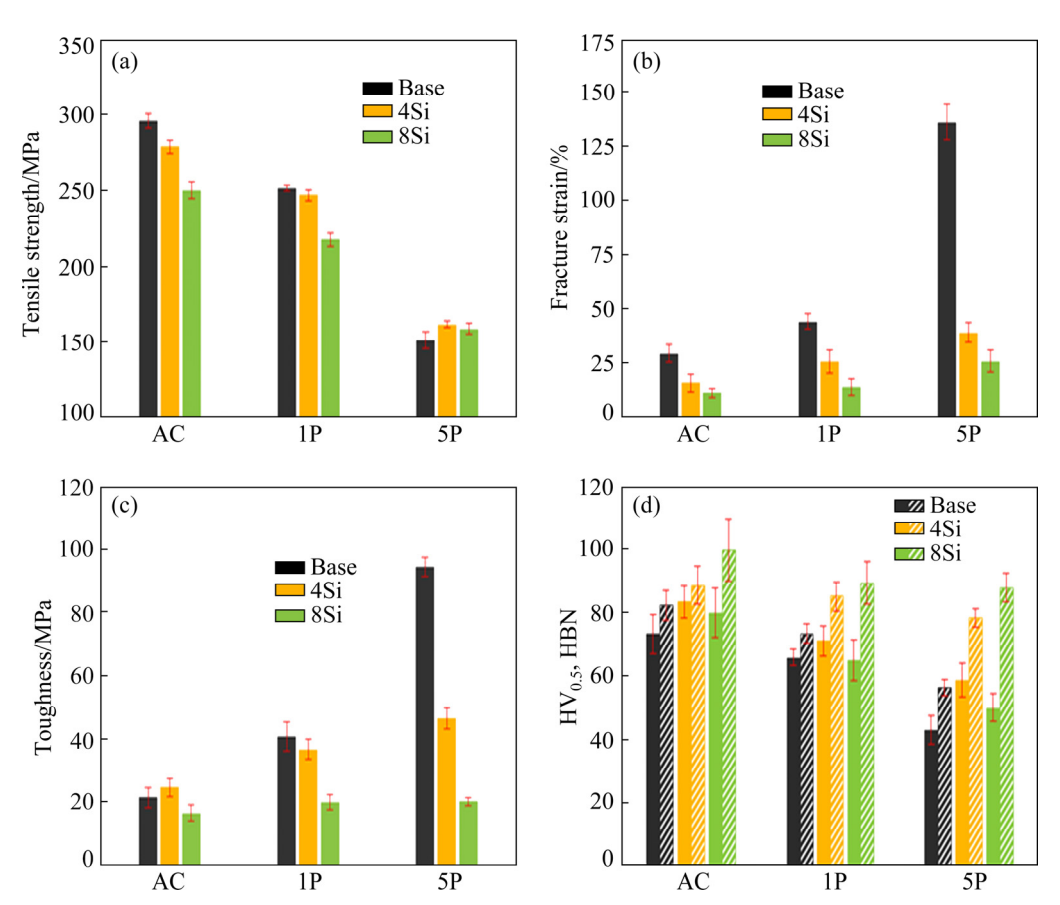


Fig. 5 Effect of number of MDF passes on mechanical properties of experimental samples; (a) Tensile strength; (b) Fracture strain; (c) Toughness; (d) Hardness (The solid and hatched bars indicate $HV_{0.5}$ and HBN, respectively)

According to the microstructural examination results (Fig. 4) and in agreement with the previous studies [28–30], breakage of the initial dendritic

network and formation of well-refined/homogenized matrix consisting of hard Al-rich α -phase and soft Zn-rich η -phase can be suggested

as two influencing factors responsible for the alloy However, regarding the intensive softening. microstructural refinement in MDFed samples, it seems that there are other important determining factors for alloy softening. Indeed, due to the difficulties associated with the cross-slip and climb of dislocations in the metals with low stacking fault energy (SFE) such as Zn [31,32], the dislocation dissociation is likely to be promoted which reduces the rate of dislocation recovery [31,33]. The low value of SFE restricts the dislocation movements, but at the same time increases the density of dislocations enhancing the stored energy microstructure [34,35]. Under this circumstance, dynamic recrystallization likely occurs which increases the fraction of high angle grain boundaries (HAGBs), thereby encouraging grain boundary migration/sliding and promoting MDF-induced strain softening [34]. Moreover, the self-annealing-induced softening might also happen in ZA22 alloy a few days after MDF process [35].

The Si addition and formation of hard Si crystals in the microstructure increase the hardness of ZA22 alloys both in micro- and macro-scale, but cannot affect their decreasing trend as the number of MDF passes increases. According to Fig. 5, adding Si up to 4 wt.% hardens the base-AC alloy, which can be explained by the formation of hard Si particles (>100 KHN [36]) within its matrix (Fig. 4(c)). However, despite substantial growth in the size and volume fraction of hard Si particles within the matrix (Fig. 4(e)), increasing the Si 8 wt.% slightly content to increases macrohardness of the experimental alloys, causes a relative reduction in their microhardness (Fig. 5(d)). This is probably due to the formation of primary Si agglomerates within the matrix which increases the interspacing of Si particles, resulting in weaker inhibition of dislocation motion [37]. Moreover, due to the blockage of possible feeding paths between the particles, the volume fraction of micropores in those regions increases (Fig. 4(e)).

3.3 Tribological properties

The effect of Si addition and multi-pass MDF on the dry sliding wear resistance of the experimental samples worn at three applied loads of 10, 20, and 30 N is shown in Fig. 6. As seen, irrespective of the applied load the highest wear resistance in the as-cast samples is observed in the

alloys containing 4 wt.% Si. It is also evident that applying MDF improves the wear resistance of the alloys, especially the Si-containing samples. For instance, at the applied load of 30 N, the wear rate of 4Si-5P sample is lower than that of 4Si-AC and base-AC samples by approximately 50% and 70%, respectively.

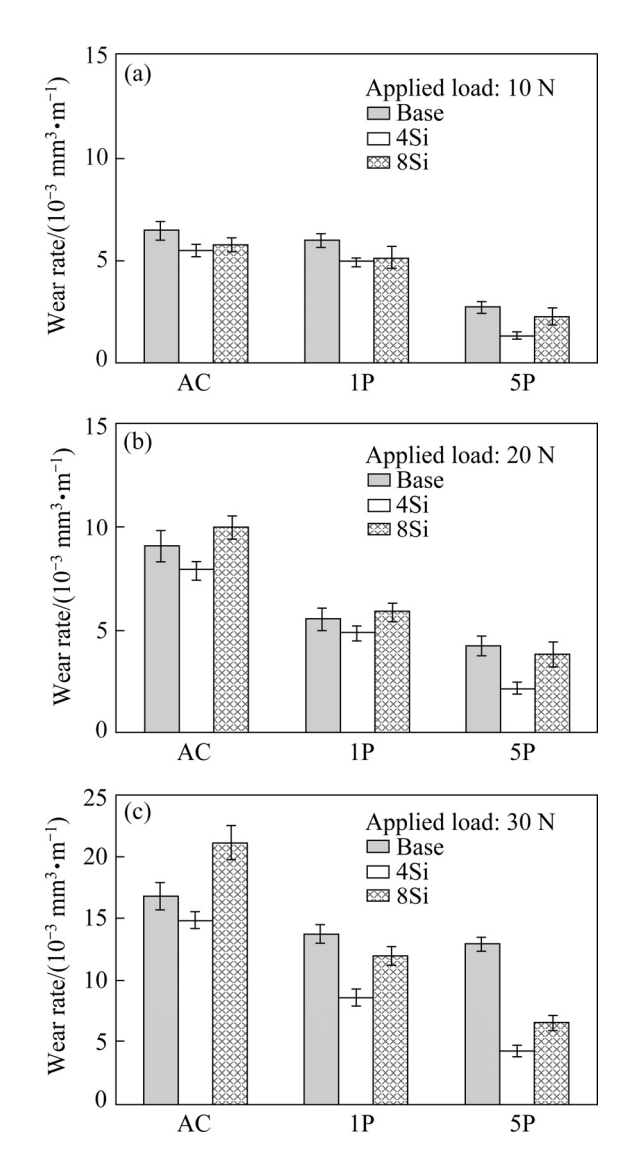


Fig. 6 Effect of applied load on wear rate of experimental alloys: (a) 10 N; (b) 20 N; (c) 30 N

In order to better understand the effect of MDF on the wear behavior of the experimental alloys, worn surfaces, size and morphology of the wear debris collected at the end of wear tests, and worn subsurface microstructures were examined. Figure 7 shows the worn surface of base-AC and base-5P samples tested at the applied loads of 10 and 30 N. The EDS analysis results (Fig. 8) confirm the formation of oxide-rich tribolayer on all worn

surfaces. The presence of oxides is an indicator of the oxidative wear (i.e. formation, oxidation, sintering, and compaction of fine loose wear particles) as one of the main wear mechanisms in these samples. Moreover, the formation of craters/pits and the presence of abrasion grooves on the worn surfaces show the delamination and abrasive wear as the other operative wear mechanisms. Considering the surface damage severity (the depth and size of craters/pits and abrasion tracks), it seems that, at the applied load of 10 N, both samples are in the mild wear regime. However, at the applied load of 30 N, base-AC and, to some extent, base-5P samples are seemingly in the severe wear regime. Increasing the depth and size of delamination craters (Fig. 7(b)) and generation of large plate-like wear particles (Fig. 9(a)) are the indications that imply severe wear of base-AC sample. In agreement with the above results, the lower concentration of oxygen in the analysis of Region C in Fig. 7(b) (Fig. 8(c)) confirms the local detachment of the tribolayer from the worn surface of base-AC sample. Moreover, the local surface deformation of base-5P sample is an important morphological feature implying the local occurrence of severe wear.

According to the wear results (Fig. 6), applying MDF improves the wear resistance of ZA22 alloy, especially at low applied loads. For instance, at the applied load of 10 N, the wear rate of base-5P sample is lower than that of base-AC sample by about 58%. Moreover, the wear resistances of base alloy at the applied loads of 20 and 30 N were improved by about 53% and 23%, respectively. The worn subsurface microstructures of base-AC and base-5P samples tested at the applied load of 30 N are shown in Fig. 10. Figure 11 also shows the variation of subsurface equivalent strain (ε) of the experimental samples, obtained by Eq. (2), against the depth below the worn surface.

$$\varepsilon = \frac{\sqrt{3}}{3} \tan \varphi \tag{2}$$

where φ is the shear angle between the grain

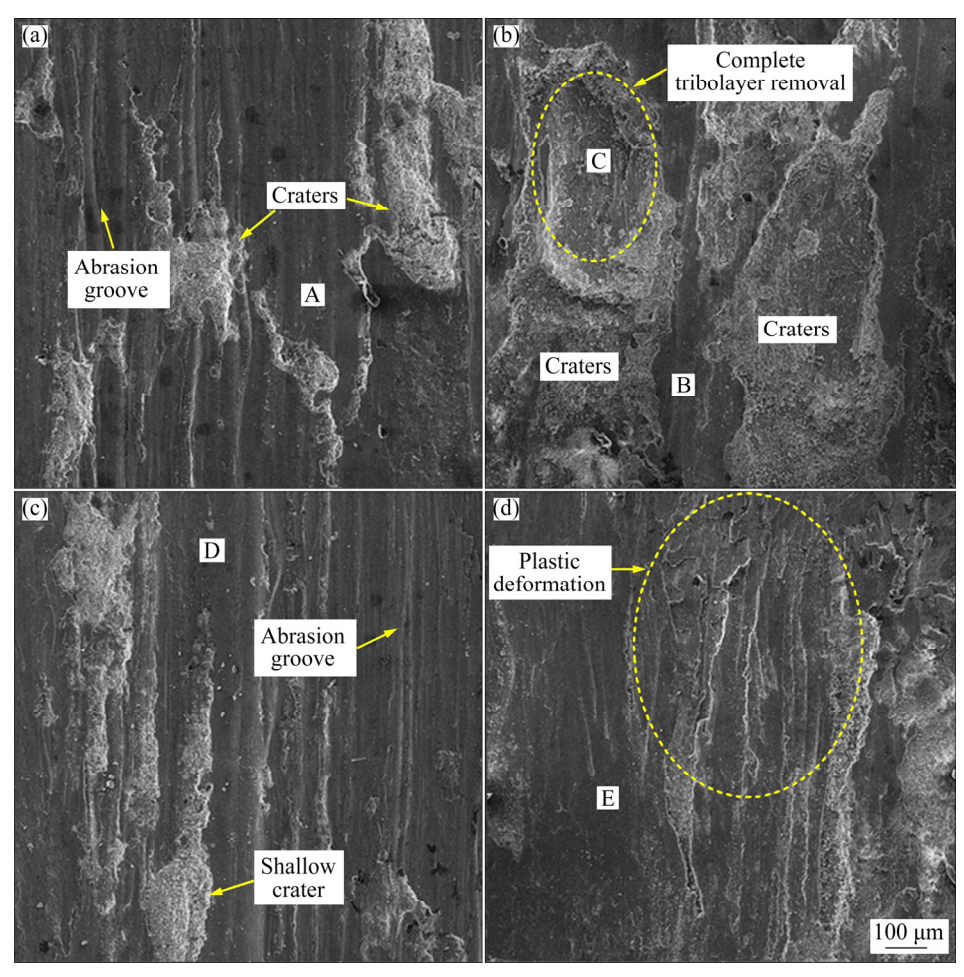


Fig. 7 Worn surface morphologies of base-AC (a, b) and base-5P (c, d) samples at applied loads of 10 N (a, c) and 30 N (b, d)

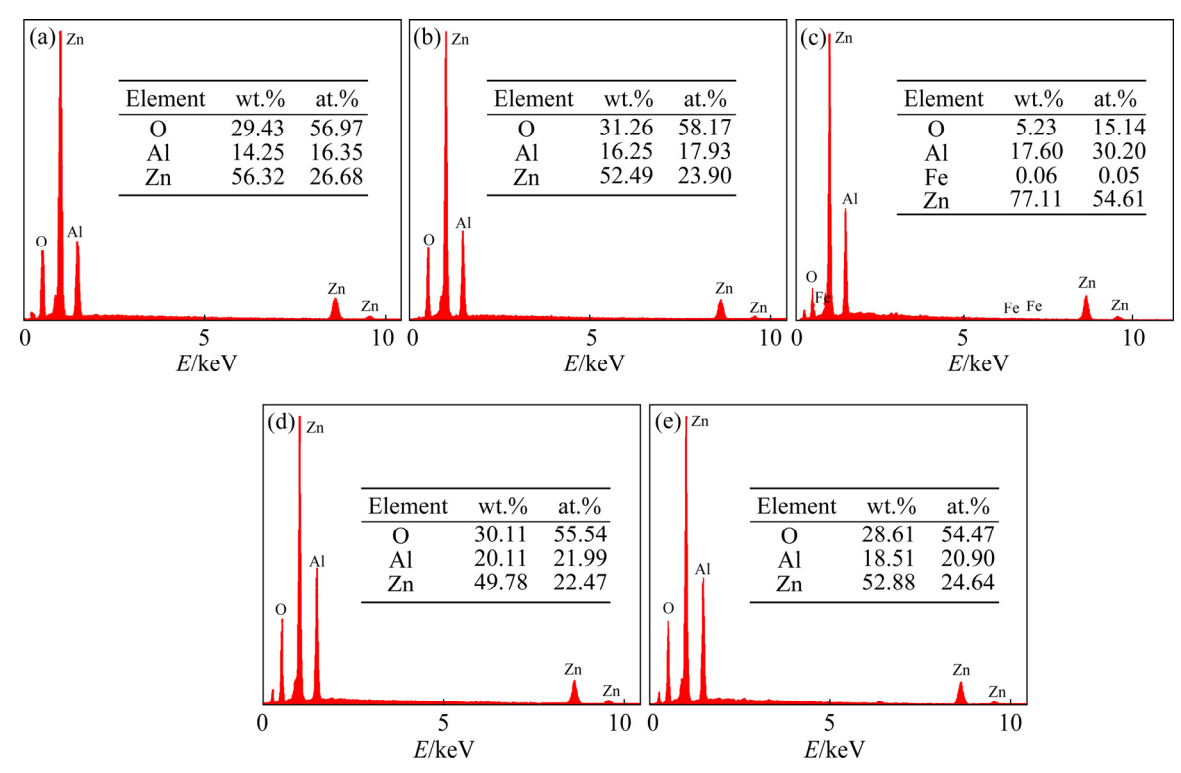


Fig. 8 EDS analyses of marked regions shown in Fig. 7: (a) Region A; (b) Region B; (c) Region C; (d) Region D; (e) Region E

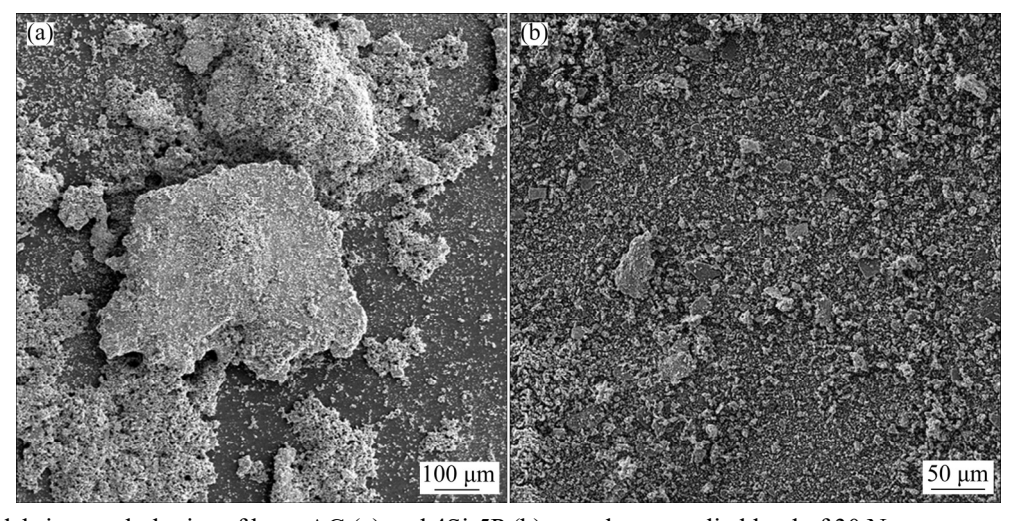


Fig. 9 Wear debris morphologies of base-AC (a) and 4Si-5P (b) samples at applied load of 30 N

boundaries and the normal direction to the worn surface [38]. As seen, as a result of substrate work-softening (Fig. 5), the depth and amplitude of subsurface deformation in MDFed samples have increased in a way that at the applied load of 30 N the depth of friction-induced deformation in base-5P sample is 53% higher than that in base-AC sample.

When the substrate hardness/strength is reduced, its potential in supporting the tribolayer is usually deteriorated, making it unstable on the worn

surface. Therefore, the reduction of the wear resistance is usually expected. However, it was found that [39] the matrix ductility also plays an important role in the wear behavior of alloys. Moreover, according to HORNBOGEN [40], if the amplitude of sliding-induced strains exceeds the critical strain at which microcracks are propagated, the wear volume becomes highly dependent on the toughness. Therefore, it seems that the better wear behavior of base-5P sample, despite its softening, is related to the improved matrix toughness (Fig. 5(c))

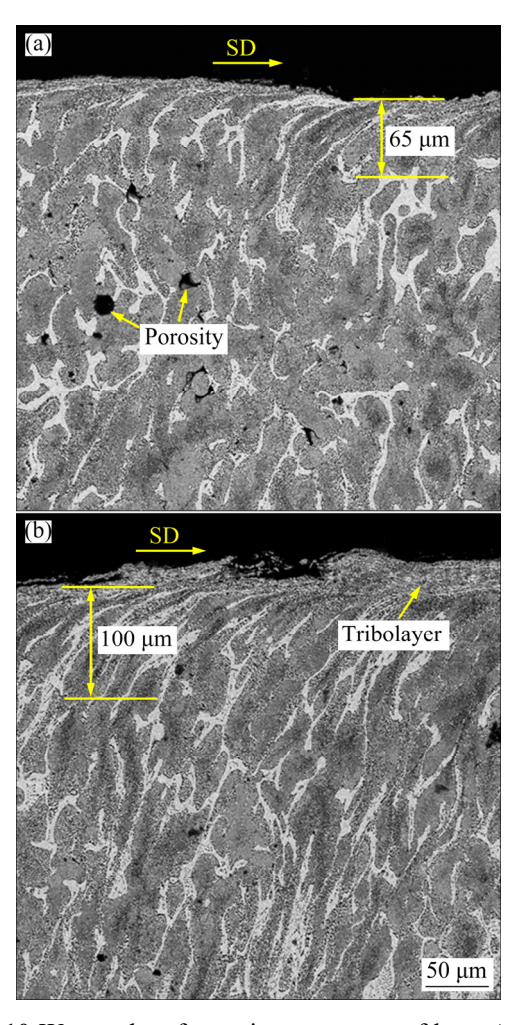


Fig. 10 Worn subsurface microstructures of base-AC (a) and base-5P (b) samples at applied load of 30 N (SD-Sliding direction)

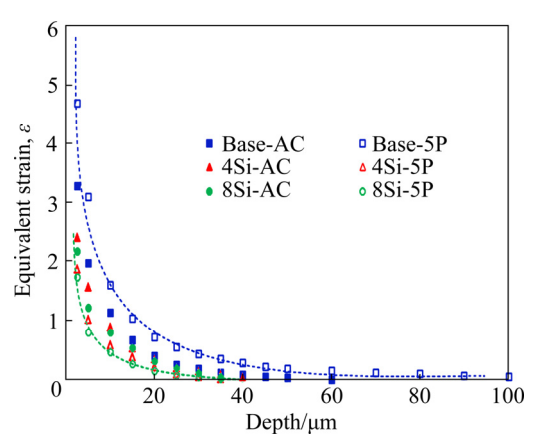


Fig. 11 Variation of subsurface equivalent strain against depth below worn surface of experimental samples (applied load of 30 N)

or equivalently its better resistance against wearinduced microcracks propagation. In addition, lower volume fraction of micropores in base-5P sample and effective mechanical intermixing of hard $\alpha+\eta$ lamellar eutectoid colonies with the average hardness of $(69.5\pm6.4)\,\mathrm{HV}_{0.02}$ and soft phase with the average hardness (47.8 ± 7.2) HV_{0.02} can be regarded as the other factors responsible for better wear properties of base-5P sample. It is worth underlining that, due to its higher thermal stability arising from its higher Al content, and its good work-hardening capability, arising from its FCC crystal structure, the α -phase contributes significantly to improving tribological behavior of ZA22 alloy. On the other hand, the Zn-rich η -phase, due to its HCP crystal structure, has great smearing characteristics, serving as a solid lubricant and a load-bearing element [38,30,41].

According to Fig. 6, adding Si decreases the wear rate of ZA22 alloy. The mechanisms by which Si enhances sliding wear behavior of Zn-Al-based alloys have been discussed elsewhere [1,3,42]. The primary particles act as hard in-situ reinforcements within the matrix of ZA alloys, which improves their overall hardness, increases their load bearing/energy absorbing capacity, and enhances their thermal stability to better resist against frictional heating. Therefore, their presence expectedly enhances the substrate resistance against sliding-induced shear strains. Figure 12 shows the subsurface microstructure and Fig. 11 shows the subsurface equivalent strain below the worn surface of 4Si-AC and 8Si-AC samples, respectively (applied load 30 N). It is evident that, compared to base-AC sample (Fig. 10), the presence of hard Si reinforcements decreases the depth/amplitude of subsurface plastic deformation.

However, in order to serve as effective reinforcements/load-bearing elements, the brittle Si particles must be well refined (to preserve their structural integrity) and evenly distributed within the matrix. Otherwise, if being subjected to the intensive surface strains, Si particles are likely to promote surface microcracking, encouraging tribolayer delamination (Fig. 13). Meanwhile, the fractured Si particles can gradually locate onto the tribolayer, decreasing its strength/integrity and encouraging the abrasive wear. The subsurface microstructures of 4Si-5P and 8Si-5p samples tested at the applied load of 30 N are shown in Figs. 12(b) and (d), respectively. As seen, the well-refined Si particles present in the substrate of these samples

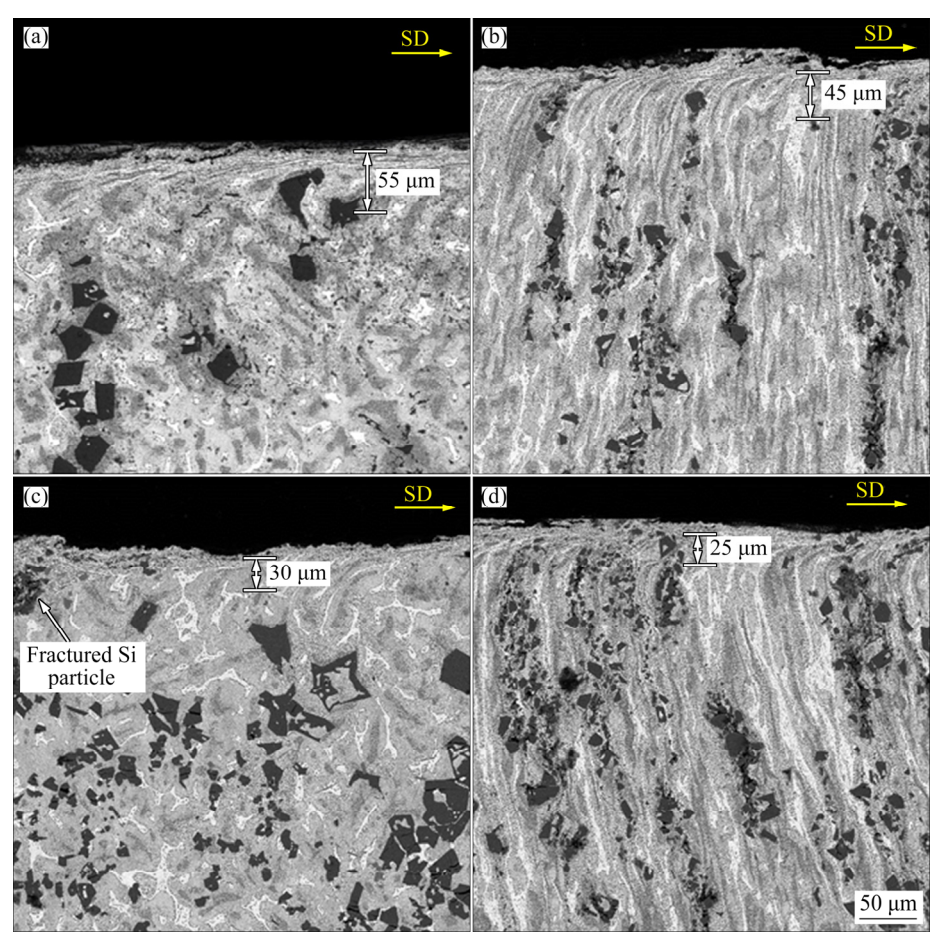


Fig. 12 Worn subsurface microstructures of 4Si-AC (a), 4Si-5P (b), 8Si-AC (c), and 8Si-5P (d) samples at applied load of 30 N

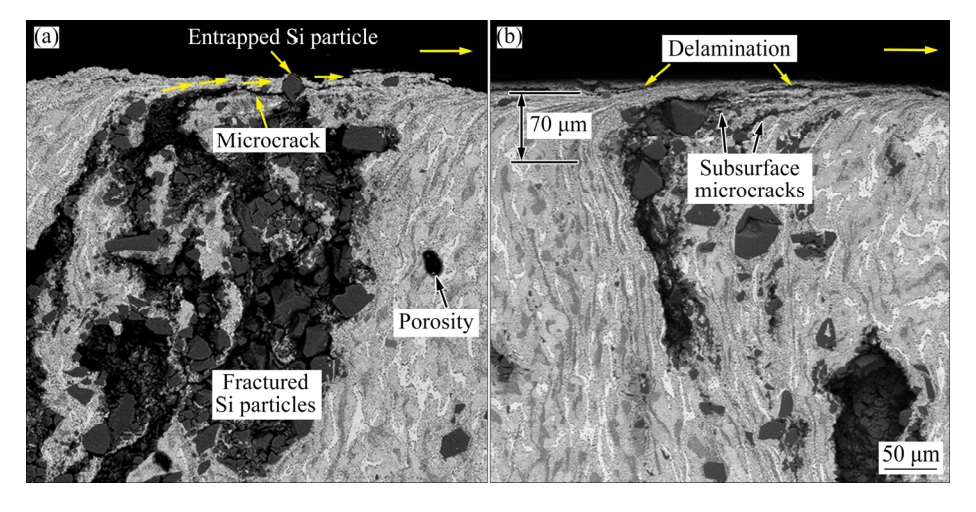


Fig. 13 SEM images showing formation of micropores and propagation of subsurface microcracks (a), and promotion of tribolayer delamination due to propagation of subsurface microcracks (b) originated from fractured Si particles in subsurface microstructure of 8Si-5P sample at applied load of 30 N

have been rotated or moved along the shear flow lines rather than being fractured maintaining their strengthening effect on the substrate. Therefore, the applied shear stresses are likely to be tolerated by a larger number of Si particles, decreasing the amplitude of stress imposed on the individual particles.

The worn surfaces of 4Si-5P and 8Si-5P samples tested at the applied loads of 10 and 30 N are shown in Fig. 14. As seen, at the applied load of

10 N, due to the strengthening effect of Si particle, the worn surfaces have been covered by a smooth and dense oxide-rich tribolayer (Fig. 15), implying the high potential of their substrate in supporting the tribolayer (Figs. 14(a) and (c)). The prominent wear mechanisms for both samples are abrasive wear and delamination under the mild wear regime.

Under the applied load of 30 N, shallow delaminated craters are observed on the worn surface of 4Si-5P sample (Fig. 14(b)), implying its operation in a mild wear regime. This can be also confirmed by the formation of high volume fractions of fine equiaxed wear particles and the small-sized plate-like wear debris (Fig. 9(b)). However, the tribolayer of 8Si-5P sample becomes highly unstable. As a result, the number/size of delaminated craters is augmented and microcracks are formed on the worn surface (Fig. 14(d)). This instability might be partly explained by the lower hardness of 8Si-5P sample ((50.1±4.4) HV_{0.5}) than that of 4Si-5P ((58.8±5.3) HV_{0.5}) mediated by its higher volume fraction of porosities. However, the

low potential of MDF process in developing a homogeneous microstructure comprising finely distributed primary Si particles seems to be the main reason for tribolayer instability in Si-rich alloys. Indeed, regardless of the fine and almost uniform distribution of the particles in most regions of 8Si-5P sample as shown in Fig. 12(d), there are some regions that, due to inefficient refinement/ distribution of Si particles, higher deformation is experienced (Fig. 13(b)), causing lower tribolayer stability and accordingly higher delamination/ abrasive wear. Moreover, according to Fig. 13, the fractured coarse Si particles or Si particle agglomerates beneath the worn surface of 8Si-5P sample facilitate surface microcracking, which further encourages the tribolayer delamination. The incorporation of Si fragments into the tribolayer, on one hand, decreases its integrity/strength and, on the other hand, promotes counterface abrasion, where the concentration of Fe and Cr elements in the worn surface composition of 8Si-5P sample is higher than that of other samples (Fig. 15(d)).

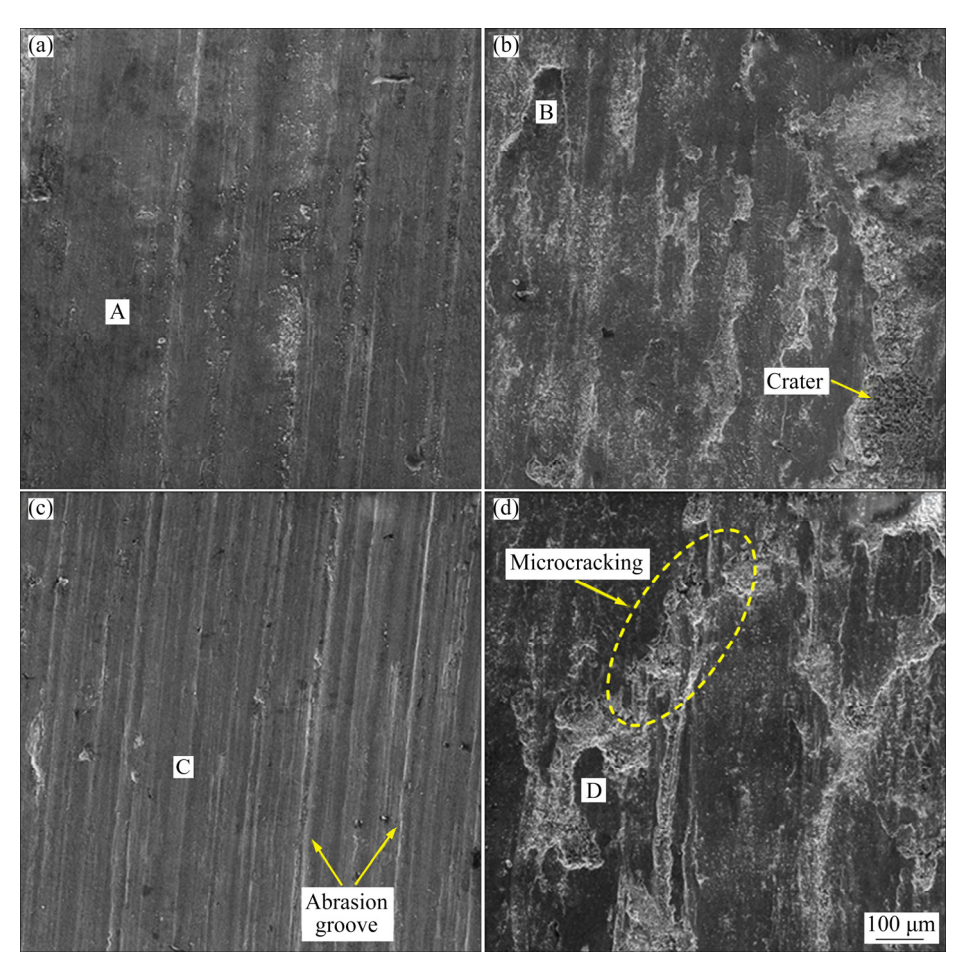


Fig. 14 Worn surface morphologies of 4Si-5P (a, b) and 8Si-5P (c, d) samples at applied loads of 10 N (a, c) and 30 N (b, d)

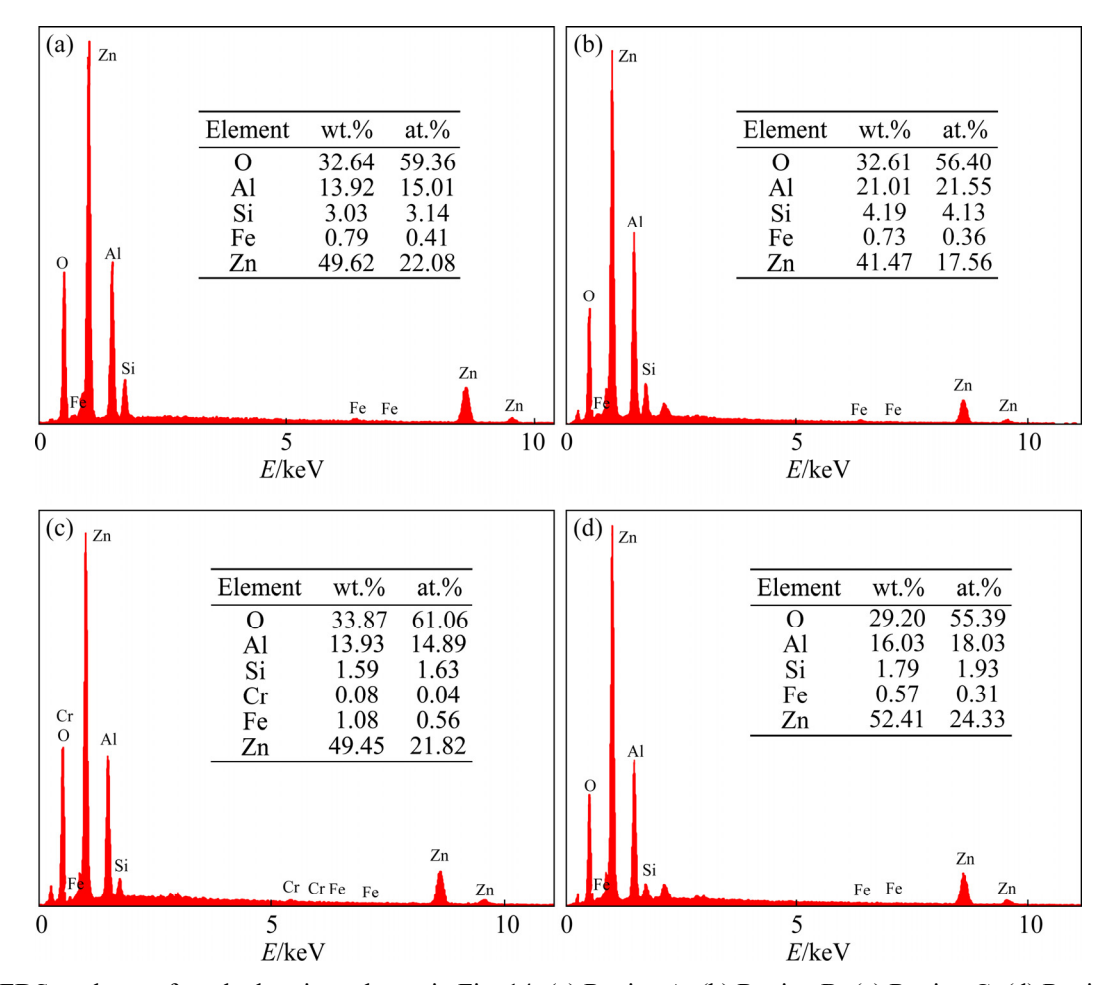


Fig. 15 EDS analyses of marked regions shown in Fig. 14: (a) Region A; (b) Region B; (c) Region C; (d) Region D

Figure 16 shows the typical friction coefficient (COF) curves for base-AC, base-5P, 4Si-AC, 4Si-5P, 8Si-AC, and 8Si-5P samples tested at the applied load of 30 N. As seen, applying MDF positively affects the friction behavior of the samples. For instance, the average friction coefficient of base-5P is lower than that of base-AC sample by 38%. Moreover, irrespective of the last 250 m of sliding, the friction coefficient curve of base-5P sample shows significantly low fluctuations.

As explained before. despite the work-softening effect of MDF on the ZA22 alloy, the improved friction behavior of base-5P sample can be mainly attributed to the microstructural densification and development of a microstructure finely-distributed comprising $\alpha + \eta$ phases. Moreover, the tribolayer formed on the worn surface of ZA alloys has a critical role in their According friction behavior. to the **EDS** microanalyses of worn surfaces, the composition of the tribolayers demonstrates high amounts of Al and Zn elements which are mainly present as their oxides. Al₂O₃, as a hard ionic compound serves as a load-bearing element in the tribolayer while ZnO, due to its open wurtzite structure, promotes self-lubrication [41]. Therefore, as long as an oxide-rich tribolayer covers the worn surface, due to a lower chance of adhesion between the interacting asperities, lower probability of debris generation and lower abrasive wear, both the average friction coefficient and friction coefficient fluctuations are low. However, when the tribolayer becomes unstable, depending on the extent to which the tribolayer is removed from the surface, the average friction coefficient and its fluctuations can increase gradually or abruptly.

In agreement with the SEM results of worn surface/subsurface (Figs. 12 and 14), adding Si reduces friction coefficient and friction coefficient fluctuation especially in the case of MDFed samples. For instance, at the applied load of 30 N, the friction coefficient of base sample decreases from 0.27±0.09 to 0.15±0.05 and 0.23±0.12 in 4Si-AC and 8Si-AC samples. Moreover, at the same

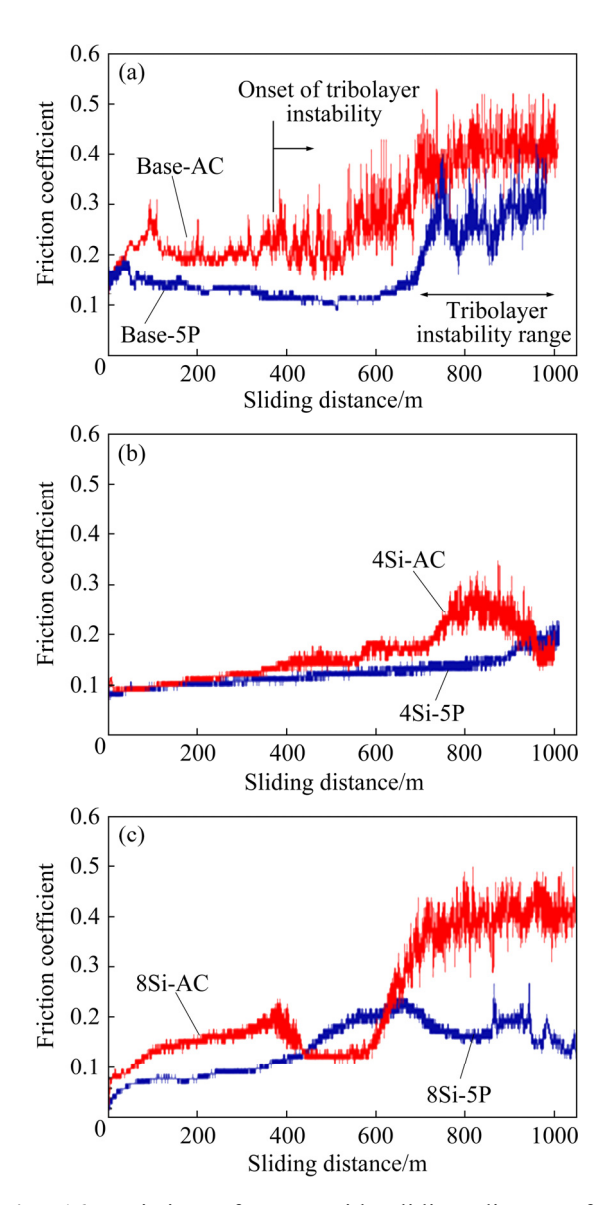


Fig. 16 Variation of COF with sliding distance for base-AC and base-5P (a), 4Si-AC and 4Si-5P (b), and 8Si-AC and 8Si-5P (c) samples (applied load of 30 N)

applied load the friction coefficients of 4Si-5P and 8Si-5P samples are lower than those of 4Si-AC and 8Si-AC samples by 20% and 43%, respectively. This improvement can be attributed to the presence of primary Si particles in the substrate of Si-containing samples, which, as hard thermally-stable reinforcements, counteract MDF-induced work-softening, thereby decreasing its plastic flow (Figs. 11 and 12) and improving its potential in supporting the tribolayer. The positive effect of Si is expected to be more pronounced at high applied loads where the frictional heating can further soften the substrate.

According to the friction coefficient curves,

the wear results (Fig. 6), and morphological studies of the worn surfaces (Fig. 14), wear debris (Fig. 9), and subsurface regions (Fig. 12), the optimum friction behavior is observed in samples containing 4 wt.% Si. However, increasing the Si content to 8 wt.%, even in the case of five-pass MDFed samples, leads to the tribolayer instability and promotes severe delamination and extensive debris generation. Moreover, the hard Si fragments entrapped on the tribolayer can promote the two-body and/or three-body abrasive wear. The aforementioned phenomena all together responsible for increasing the friction and chaotic fluctuations in friction coefficient curve (Fig. 16(c)).

4 Conclusions

- (1) MDF breaks down the initial dendritic network, effectively refines α and η -phases and Si particles (in Si-containing alloys), improves the distribution of different phases within the matrix, and decreases the volume fraction of micropores. The average size of primary Si particles decreases from 25 and 30.4 μ m in 4Si-AC and 8Si-AC alloys to less than about 8.1 and 7.3 μ m in 4Si-5P and 8Si-5P alloys, respectively.
- (2) Increasing the number of MDF passes progressively softens the alloys while improving their ductility and toughness. According to the mechanical properties results, the hardnesses of base-5P, 4Si-5P, and 8Si-5P samples are lower than those of base-AC, 4Si-AC, and 8Si-AC samples by 41%, 30%, and 37%, respectively. Moreover, the toughnesses of base-AC, 4Si-AC, and 8Si-AC samples increase after five-pass MDF by about 350%, 90%, and 20%, respectively.
- (3) MDF can improve the tribological properties of ZA22–xSi alloys. For instance, at the applied load of 30 N, the wear rate and average friction coefficient of 4Si-5P sample are lower than those of 4Si-AC and base-AC samples by 70% and 75%, and 20% and 54%, respectively. The fine distribution of α and η -phases, the presence of hard Si reinforcements in the microstructure, and the presence of Al and Zn oxides in the tribolayer composition which, respectively, act as load-bearing and self-lubricating elements, can be considered as the main factors, improving the wear and friction behavior.

References

- [1] SAVAŞKAN T, BICAN O. Effects of silicon content on the microstructural features and mechanical and sliding wear properties of Zn-40Al-2Cu-(0-5)Si alloys [J]. Materials Science and Engineering A, 2005, 404: 259-269.
- [2] SAVAŞKAN T, ANVARI MALEKI A. Friction and wear properties of Zn-25Al-based bearing alloys [J]. Tribology Transactions, 2014, 57: 435-444.
- [3] LEE P P, SAVAŞKAN T, LAUFER E. Wear resistance and microstructure of Zn–Al–Si and Zn–Al–Cu alloys [J]. Wear, 1987, 117: 79–89.
- [4] KUMAR P, WANI M F. Tribological characterization of hypereutectic Al–25Si alloy under dry and lubricated sliding conditions [J]. Journal of Tribology, 2018, 140: 011603.
- [5] AKBARI M, SHOJAEEFARD M H, ASADI P, KHALKHALI A. Wear performance of A356 matrix composites reinforced with different types of reinforcing particles [J]. Journal of Material Engineering and Performance, 2017, 26: 4297–4310.
- [6] LOZANO D E, MERCADO-SOLÍS R D, JUAREZ-HERNANDEZ A, HERNÁNDEZ-RODRÍGUEZ M A L, GARZA-MONTES-DE-OCA N F. Wear mechanisms experienced by an automotive grade Al-Si-Cu alloy under sliding conditions [J]. Ingenieria Mecánica Technologia Y Desarrolldollo, 2015, 5: 339-345.
- [7] GUTIÉRREZ-MENCHACA, J, TORRES-TORRES, D, GARAY-TAPIA, A M. Microstructural, mechanical and thermodynamic study of the as-cast Zn–Al–Sr alloys at high Sr content [J]. Journal of Alloys and Compounds, 2020, 829: 154511.
- [8] DORANTES-ROSALES H J, LÓPEZ-HIRATA V M, ESQUIVEL-GONZÁLEZ R, GONZÁLEZ-VELAZQUEZ J L, MORENO-PALMERIN J, TORRES-CASTILLO A. Zn-22Al-2Cu alloy phase transformations at different homogenizing temperatures [J]. Metals and Materials International, 2012, 18(3): 385-390.
- [9] YOUSEFI, D, TAGHIABADI, R, SHAERI, M H, ANSARIAN, I. Microstructural evolution and mechanical properties of multi-directionally forged SiP/ZA22 composite [J]. Archives of Civil and Mechanical Engineering, 2020. https://doi.org/10.1007/s43452-020-00124-z.
- [10] MICHALIK, R. Influence of heat treatment on phase composition and structure of ZnAl40Cu(1-2)Ti(1-2) alloys [J]. Institute of Metallurgy and Materials Science of Polish Academy of Sciences, 2018, 63(1): 461-466. https://doi.org/ 10.24425/118962.
- [11] BERENT K, PSTRUŚ J, GANCARZ T. Thermal and microstructure characterization of Zn-Al-Si alloys and chemical reaction with Cu substrate during spreading [J]. Journal of Materials Engineering and Performance, 2016, 25: 3375-3383.
- [12] HERLACH D M, SIMONS D, PICHON P Y. Crystal growth kinetics in under cooled melts of pure Ge, Si and Ge–Si alloys [J]. Philosophical Transactions of the Royal Society A: Mathematical, Physical and Engineering Sciences, 2018, 376: 20170205.

- [13] WANG R Y, LU W H, HOGAN L M. Faceted growth of silicon crystal in Al–Si alloys [J]. Metallurgical and Materials Transactions A, 1997, 28: 1233–1243.
- [14] PRASAD B K. Effects of partially substituting copper by silicon on the physical, mechanical, and wear properties of a Zn-37.5%Al-based alloy [J]. Materials Characterization, 2000, 44: 301-308.
- [15] LIU Y, YANG G, LU Y, YANG L. Damping behavior and tribological properties of as-spray-deposited high silicon alloy ZA27 [J]. Journal of Materials Processing and Technology, 1999, 87: 53–58.
- [16] ZHU Q, LI L, BAN C, ZHAO Z, ZUO Y, CUI J. Structure uniformity and limits of grain refinement of high purity aluminum during multi-directional forging process at room temperature [J]. Transactions of Nonferrous Metals Society of China, 2014, 24(5): 1301–1306.
- [17] NIE K, ZHU Z, MUMROE P, DENG K, GUO Y. Microstructure and mechanical properties of TiC nanoparticle-reinforced Mg–Zn–Ca matrix nanocomposites processed by combining multidirectional forging and extrusion [J]. Transactions of Nonferrous Metals Society of China, 2020, 30(9): 2394–2412.
- [18] ANJAN B N, KUMAR G V P. Microstructure and mechanical properties of ZA27 based SiC reinforced composite processed by multi directional forging [J]. Materials Research Express, 2018, 5: 106523.
- [19] ANSARIAN I, SHAERI M H, EBRAHIMI M, MINÁRIK P, BARTHA K. Microstructure evolution and mechanical behaviour of severely deformed pure titanium through multi directional forging [J]. Journal of Alloys and Compounds, 2019, 776: 83–95.
- [20] HUANG H, ZHANG J. Microstructure and mechanical properties of AZ31 magnesium alloy processed by multidirectional forging at different temperatures [J]. Materials Science and Engineering A, 2016, 674: 52–58.
- [21] ZHU Q F, LEI L I, BAN C Y, ZHAO Z H, ZUO Y B, CUI J Z. Structure uniformity and limits of grain refinement of high purity aluminum during multi-directional forging process at room temperature [J]. Transactions of Nonferrous Metal Society of China, 2014, 24: 1301–1306.
- [22] SHARATH P C, UDUPA K R, KUMAR G V P. Effect of multi directional forging on the microstructure and mechanical properties of Zn-24wt.%Al-2wt.%Cu alloy [J]. Transactions of the Indian Institute of Metals, 2017, 70: 89-96.
- [23] MIURA H, YU G, YANG X, SAKAI T. Microstructure and mechanical properties of AZ61 Mg alloy prepared by multi directional forging [J]. Transactions of Nonferrous Metals Society of China, 2010, 20(7): 1294–1298.
- [24] da SILVA N A N, PEREIRA P H R, SIQUEIRA CORRÊA E C, PAULINO AGUILAR M T, CETLIN P R. Microstructural evolution and mechanical properties in a Zn-Al-Cu-Mg hypoeutectic alloy processed by multi-directional forging at room temperature [J]. Materials Science and Engineering A, 2021, 801: 140420, https://doi.org/10.1016/j.msea.2020. 140420.
- [25] HUBBARD J L. Microscopy and image analysis, materials Handbook [M]. 9th ed, Vol. 7. Ohio: American Society for Metals, Materials Park, 1996: 225–230.

809-820

- [26] TAYLOR R P, MCCLAIN S T, BERRY J T. Uncertainty analysis of metal-casting porosity measurements using Archimedes' principle [J]. International Journal of Cast Metals Research, 1999, 11: 247–257.
- [27] YOUSEFI D, TAGHIABADI R, SHAERI M H, ABEDINZADEH P. Enhancing the mechanical properties of Si particle reinforced ZA22 composite by Ti-B modification [J]. International Journal of Metalcasting, 2021, 15: 206-215.
- [28] BABIC M, MITROVIC S, NINKOVIC R. Tribological potential of zinc-aluminium alloys improvement [J]. Tribology in Industry, 2009, 31: 15–28.
- [29] VILLEGAS-CARDENAS J D, SAUCEDO-MUÑOZA M L, LOPEZ-HIRATAA V M, DORANTES-ROSALESA H J, GONZALEZ-VELAZQUEZA J L. Effect of phase transformations on hardness in Zn-Al-Cu Alloys [J]. Materials Research, 2014, 17: 1137-1144.
- [30] HERNÁNDEZ-RIVERA J L, FLORES E E M, CONTRERAS E R, ROCHA J G, de JESUS CRUZ-RIVERA J, TORRES-VILLASEÑOR G. Evaluation of hardening and softening behaviors in Zn–21Al–2Cu alloy processed by equal channel angular pressing [J]. Journal of Materials Research and Technology, 2017, 6(4): 329–333.
- [31] HU Q M, YANG R. Basal-plane stacking fault energy of hexagonal close-packed metals based on the Ising model [J]. Acta Materialia, 2013, 61: 1136–1145.
- [32] ROY B, DAS J. Strengthening face centered cubic crystals by annealing induced nano-twins [J]. Scientific Reports, 2017, 7(1): 17512. https://doi.org/10.1038/s41598-017-17848-3.
- [33] BALOGH L, UNGA'R T, ZHAO Y, ZHU Y T, HORITA Z, XU C, LANGDON T G, Influence of stacking-fault energy on microstructural characteristics of ultrafine-grain copper and copper–zinc alloys [J]. Acta Materialia, 2008, 56:

- [34] EDALATI K, HASHIGUCHI Y, IWAOKA H, MATSUNAGA H, VALIEV R Z, HORITA Z, Long-time
- MATSUNAGA H, VALIEV R Z, HORITA Z, Long-time stability of metals after severe plastic deformation: Softening and hardening by self-annealing versus thermal stability [J]. Materials Science and Engineering A, 2018, 729: 340–348.
- [35] XIAN Z N, KAWASAKI M, HUANG Y, LANGDON T G. The significance of self-annealing in two-phase alloys processed by high-pressure torsion [C]//6th International Conference on Nanomaterials by Severe Plastic Deformation, IOP Conference Series: Materials Science and Engineering, 2014. 63: 012126.
- [36] TENEKEDJIEV N, GRUZLESKI J E. Hypereutectic aluminium—Si casting alloys—A review [J]. Cast Metals, 1990, 3: 96–105.
- [37] YINGYING S, MIN S, YUEUI H. Effects of Sc content on the mechanical properties of Al–Sc alloys [J]. Rare Metals, 2010, 29: 451–454.
- [38] PERRIN C, RAINFORTH W M. Work hardening behavior at the worn surface of Al–Cu and Al–Si alloys [J]. Wear, 1997, 203–204: 171–179.
- [39] LU Z C, ZENG M Q, GAO Y, ZHU M. Minimizing tribolayer damage by strength–ductility matching in dual-scale structured Al–Sn alloys: A mechanism for improving wear performance [J]. Wear, 2013, 304: 162–172.
- [40] HORNBOGEN E. The role of fracture toughness in the wear of metals [J]. Wear, 1975, 33: 251–259.
- [41] PÜRÇEK G, SAVAŞKAN T, KÜÇÜKÖMERO GLU T, MURPHY S. Dry sliding friction and wear properties of zinc-based alloys [J]. Wear, 2002, 252: 894–901.
- [42] RAJABI F, TAGHIABADI R, SHAERI M H. Tribology of Si-rich TIG-deposited coatings on Zn-40Al-2Cu alloy [J]. Surface Engineering, 2020, 36(7): 735-744. https://doi.org/10.1080/02670844.2020.1728909.

多道次多向锻造对富硅共析 ZA 合金摩擦性能的影响

D. YOUSEFI, R. TAGHIABADI, M. H. SHAERI

Department of Materials Science and Metallurgy, Imam Khomeini International University, Qazvin, Iran

摘 要:研究多道次多向锻造(MDF)对 ZA22-xSi (x=0, 4, 8, 质量分数,%)合金摩擦性能的影响。结果表明,MDF 破坏合金的铸造组织,形成由细小分布的 α 相和 η 相,以及原始 Si 颗粒组成的显微组织。研究还发现,尽管基体出现加工软化,多向锻造 ZA22-xSi 合金仍具有较高的耐磨性。经 5 道次多向锻造的 ZA22-xSi 合金具有最高的耐磨性能,当外加载荷为 10 和 30 N 时,其磨损率分别比铸态 ZA22 合金的低 80%和 75%。MDF 也显著降低样品的平均摩擦因数和摩擦因数波动。摩擦性能提高的主要因素有:基体具有较高的抗微裂纹能力,硬质 Si 增强相的形成,显微组织中细小的 α 相和 η 相再分布,以及富 Al 和 Zn 氧化物摩擦层。

关键词: 多向锻造(MDF); Zn-22Al 合金; 硅; 摩擦学

(Edited by Xiang-qun LI)